DRAFT VERSION SEPTEMBER 30, 2009
Preprint typeset using LaTeX style emulateapj v. 04/20/08

DISK GALAXIES WITH BROKEN LUMINOSITY PROFILES FROM COSMOLOGICAL SIMULATIONS

F.J. MARTÍNEZ-SERRANO, A. SERNA, M. DOMENÉCH-MORAL
Depto. de Física y A.C., Universidad Miguel Hernández, E-03202 Elche, Alicante, Spain

AND

R. DOMÍNGUEZ-TENREIRO
Depto. de Física Teórica, Universidad Autónoma de Madrid, E-28049 Cantoblanco, Madrid, Spain

Draft version September 30, 2009

ABSTRACT

We present SPH cosmological simulations of the formation of three disk galaxies with a detailed treatment of chemical evolution and cooling. The resulting galaxies have properties compatible with observations: relatively high disk-to-total ratios, thin stellar disks and good agreement with the Tully-Fisher and the luminosity-size relations. They present a break in the luminosity profile at 3.0 ± 0.5 disk scale lengths, while showing an exponential mass profile without any apparent breaks, in line with recent observational results. Since the stellar mass profile is exponential, only differences in the stellar populations can be the cause of the luminosity break. Although we find a cutoff for the star formation rate imposed by a density threshold in our star formation model, it does not coincide with the luminosity break and is located at 4.3 ± 0.4 disk scale lengths, with star formation going on between both radii. The color profiles and the age profiles are "U-shaped", with the minimum for both profiles located approximately at the break radius. The SFR to stellar mass ratio increases until the break, explaining the coincidence of the break with the minimum of the age profile. Beyond the break we find a steep decline in the gas density and, consequently, a decline in the SFR and redder colors. We show that most stars (64-78%) in the outer disk originate in the inner disk and afterwards migrate there. Such stellar migrations are likely the main origin of the U-shaped age profile and, therefore, of the luminosity break.

Subject headings: galaxies: formation — galaxies: evolution — galaxies: spiral — galaxies: stellar content — methods: N-body simulations

1. INTRODUCTION

There is a growing body of observations that show that the classical picture of spiral galaxies with a purely exponential disk does not match most galaxies found in the local (Pohlen et al. 2002; Pohlen & Trujillo 2006; Pohlen et al. 2007; van der Kruit 2007; Bakos et al. 2008) or distant universe (Pérez 2004; Trujillo & Pohlen 2005; Azzollini et al. 2008). Indeed, galactic disks with a single exponential surface brightness profile (Type-I, in the classification of Freeman 1970) are relatively rare ($\lesssim 15\%$). Most profiles are better fitted by two exponentials separated at a well defined break radius, with the outer exponential being either downbending (Type-II, the majority) or upbending (Type-III, first discovered by Erwin et al. 2005). The profiles with an upbending break could be explained (Pohlen & Trujillo 2006, PT06 hereafter) either from a disturbed morphology due to interactions with neighboring galaxies or, in some cases, by the presence of an $R^{1/4}$ bulge component that rises over the exponential disk in the outer region. The origin of Type-II profiles, more frequent in late-type galaxies, is instead much more poorly understood.

Several authors have investigated how galaxy disks develop a downbending break, mainly through non-cosmological N-body simulations of isolated objects (Debattista et al. 2006; Bournaud et al. 2007; Roškar et al. 2008a,b; Foyle et al. 2008), but also from cosmological simulations (Abadi et al. 2003; Governato et al. 2007). All these works agree in explaining the observed break in the surface brightness profile as the result of an intrinsic break in the mass profile for the stellar component. In the most widely considered scenario, the break in the stellar mass profile develops as a consequence of a cutoff in the star formation (Elmegreen & Parravano 1994). In such a scenario the outer exponential disk would be formed by stars that migrate from the inner disk towards the regions beyond the star formation cutoff, prompted by secular instabilities such as spiral arms (Roškar et al. 2008a,b) or clump disruptions (Bournaud et al. 2007). An alternative model has been suggested by Foyle et al. (2008) after simulations starting from an already formed single exponential disk. In their simulations the inner disk forms when the bulge draws mass from the inner regions, thus making the inner disk profile shallower while the outer region stays almost unaltered and fixed by the initial conditions.

All the above models fail however to match recent observational evidence provided by Bakos et al. (2008)[1]. These latter authors have analyzed a sample of late-spirals and found that galaxies with a Type-II surface brightness profile generally have a "U-shaped" color profile with its minimum nearly located at the luminosity break radius. When this color profile was taken into account to calculate the stellar surface mass density, they obtained almost purely exponential mass profiles. Consequently, the observed luminosity break in Type-II galaxies does not seem to be necessarily related to an intrinsic break in the stellar mass profile. A downbending of the luminosity profile could also be caused by differences between the stellar populations of the inner and outer disk, even with no breaks in the mass profile at all. However, stellar counts of RGB stars in the outskirts of M33 (Ferguson et al. 2007) or NGC 4244 (de Jong et al. 2007) indicate that this may not

Electronic address: franjesus@umh.es

[1] A work by Sanchez-Blazquez et al. (2009) appeared about the time this paper was submitted showing that, in agreement with our work, broken luminosity profiles can appear in simulated galaxies with exponential mass profiles.

always be the case.

The aim of this letter is to study whether numerical simulations can naturally predict the above observed features: downbending broken luminosity profiles in galactic disks with a purely exponential mass distribution. We will use cosmological simulations where galaxies form after the collapse of primordial instabilities and where their final structure arises from a hierarchical sequence of mass aggregation and from the interaction with their environments.

2. THE SIMULATIONS

The N-Body + SPH simulations have been performed using an OpenMP parallel version of DEVA code (Serna et al. 2003) and the methods for star formation, chemical feedback and abundance-dependent cooling described in Martínez-Serrano et al. (2008). In this code, particular attention has been paid that the conservation laws hold as accurately as possible. Star formation is implemented through a Kennincutt-Schmidt-like law with a density threshold of $\rho_{\rm thres} = 6.75 \times 10^{-26}$ g/cm^3 and a star formation efficiency of $c_* = 0.1$, that implicitly account for energy feedback[2]. Each simulation is a cosmological *zoom-in* that includes high-resolution gas and dark matter for the flow converging region that generates the main object. The rest of the simulation box is sampled by low-resolution dark matter particles that account for tidal forces over the flow converging region. As a first step we consider a concordance cosmological model and generate three high-resolution initial conditions in a box of 10 Mpc per side[3] After degrading these conditions we perform the corresponding full box simulations at lower resolution. In each of these three simulations, we selected one object (the most massive one with a prominent gas disk at $z = 0$ not clearly disrupted from a very recent major merger) and traced back the particles inside its virial radius until the initial redshift z_{init}. We then computed the convex hull (Barber et al. 1996) enclosing these particles at z_{init} and substituted all the particles inside the convex hull by their high resolution counterparts. Gas particles outside the hull are eliminated and their masses added to the low-resolution dark matter component, thus obtaining the initial conditions for each simulation. The galaxies obtained in this way have a full history of mergers and accretion in a cosmological context, without any assumptions made for their initial conditions beyond the cosmology and the initial conditions generator used (Prunet et al. 2008). The mass resolution for baryonic particles used in each simulation is specified in Table 1.

3. DISK OBJECT PROPERTIES

3.1. *Consistency with observational data*

Object properties are summarized in Table 1, where we can see a remarkable consistency with observational data (Fig. 1 displays their face-on and edge-on images). They span a range of stellar masses from 1.71 to 3.86 $\times$ 10^{10} M$_\odot$. Their luminosity profiles have been obtained and fitted by following the procedures described in §3.2 below (see also the notes of Table 1). A first remarkable feature of our simulations is that we obtain objects with bulge sizes comparable to those recently obtained by Governato et al. (2008). Indeed, two out of the three simulated objects have D/T ratios implying rather small bulges, consistent with those observed for late-type spirals (*e.g.* Balcells et al. 2007; Gadotti 2009). This is an interesting property because, although Type-II breaks appear in all spiral types, they are more abundant in late Hubble types (PT06, Erwin et al. 2008). Note also that the disks are rather thin with vertical scales of $\sim 0.4 - 0.6$ kpc for the thin disk and $\sim 1.5 - 2.2$ kpc for the thick disk. We also display in Table 1 the I-band absolute magnitude and the gas rotation velocity of each object. They are found to be in good agreement with the observed Tully-Fisher relation (*e.g.* Giovanelli et al. 1997; Springob et al. 2007, see Fig. 6 of the latter reference). In the same way, through Sérsic fits to the total light distribution we have determined the r-band absolute Sérsic magnitude $M_{r,s}$ and the half-light radius $r_{50,s}$ (see Table 1). The obtained values are again in good agreement with both the luminosity-size and stellar mass-size relations for disk galaxies given by Shen et al. (2003) (see their Figs. 6 and 11, respectively).

3.2. *Broken face-on profile*

In the first row of Fig. 2 we plot the azimuthally averaged surface luminosity profiles in both the g and r bands for the three simulated galaxies, along with an approximate limit surface luminosity $\mu_{\rm lim}$ beyond which SDSS observations such as those of PT06 become background-dominated. These profiles were obtained by computing the luminosity of each stellar particle, essentially a single stellar population (SSP) with known age and metallicity, and interpolating in the Bruzual & Charlot (2003) tables. We note that all these profiles can indeed be considered as broken exponentials. The slope in the outer disk region is in all cases steeper than in the inner disk and, hence, the three simulated objects can be classified as Type-II galaxies. We have then fitted each profile by means of a Levenberg-Marquardt algorithm based on a double exponential + bulge model. In order to reduce noise, the fits were computed by using the integrated luminosity profiles instead of the surface luminosity profiles. The resulting bulge and disk scale lengths are given in Table 1, as well as the break radius (defined by the intersection of the inner and outer exponentials) of each galaxy. We find that the average ratio between the break radius and the inner exponential disk scale is $r_b/r_s = 3.0 \pm 0.5$, in agreement with the value found by PT06.

We also note that the g and r profiles have different slopes, both before and after the break radius. This results in characteristic "U-shaped" g - r profiles such as those depicted in the second row of Fig. 2. These color profiles are very similar to those observed in many spiral galaxies with broken profiles (Bakos et al. 2008). The stellar mass profiles however do not show any downbending trend. On the contrary, as row 3 of Fig. 2 shows, mass profiles can be considered as Type I (no break) in all the simulated galaxies, or even with a very slightly upbending trend (Type III). This result agrees with the findings of Bakos et al. (2008) who used the M/L ratio provided by Bell et al. (2003) to derive a mass profile from observational data. In any case, outside the luminosity break we do not find any lack of stellar mass respect to a single exponential decline.

In order to progress in understanding the nature of the above downbending luminosity profiles, we have analyzed the possible connection between the break radius and the cutoff radius for star formation. In the first row of Fig. 3 we represent the surface gas density for each galaxy. For all of them the profile shows a plateau that extends from the center of the galaxy with a shallow slope until the break radius, marked with a

[2] We use this simple model for subresolution physics because our aim in this paper is to test the minimal conditions for the formation of realistic disks.

[3] Although this box side implies a lack of very massive objects and environments, it has little effect on the internal properties of the haloes (Power & Knebe 2006).

dotted vertical line. Given the Schmidt-Kennicutt star formation recipe implemented in our code (Martínez-Serrano et al. 2008), the star formation rate (SFR) is expected to follow the gas density at a power 1.5 and increase towards the centre. Indeed, in the second row we depict the instantaneous SFR at $z = 0$, which follows a similar trend, with a steeper slope, especially for $r > r_b$. On the same row it is also represented the fraction of gas particles above the density threshold for star formation, and the fraction of gas particles eligible to form stars according to both the density criterion and the convergent flow ($\nabla \cdot \mathbf{v} < 0$) criterion. As it can be seen, the density criterion effectively imposes a cutoff radius for the star formation, while the convergent flow criterion does not impose any significant restriction on the amount of gas particles able to form stars at a given radius, appearing just as some oscillations due to the spiral arm structure of the objects that compresses and rarefies the gas. The position of the $\rho_{\rm thres}$ cutoff is always well outside the break radius, implying that our choice of $\rho_{\rm thres}$ does not directly impose the position of the luminosity break, but it rather appears well within the zone where star formation is allowed. Note also that the cutoff position coincides approximately with a surface gas density (first row of Fig. 3) of ~ 1 $M_\odot/pc^2$, while the density at the break is ~ 10 $M_\odot/pc^2$, coinciding with the value given by Martin & Kennicutt (2001) for the threshold of star formation.

In the works of Roškar et al. (2008b,a), a break in the mass profile appears in the same position where a significant drop in the SFR happens, with the stars beyond the break being transported there by migrations from the inner parts of the galaxy. Our galaxies instead do not show such a steep break for the SFR and consistently do not present a break on the stellar mass profile, so that the only interpretation for this fact is a difference in the stellar populations in each region. Indeed, as row 3 of Fig. 3 shows, there is a "U-shape" profile for the mean stellar age, very similar in shape to the color profile. The break on the profile appears to be at the minimum of the stellar age profile for galaxies 6795 and 5004, while 5003 presents a larger minimum. The coincidence between the break radius and the minimum of the age profile was already noted by Roškar et al. (2008b). Given that young stellar populations are brighter than old ones, the age decrease until the break radius makes the light profile shallower than the mass profile, while the increase after the break radius makes it steeper. This fact alone would explain the luminosity break. It also readily accounts for the color profile, since younger populations are bluer.

4. ORIGIN OF THE STARS IN THE OUTER DISK AND DISCUSSION

Our interpretation of the appearance of a break in the luminosity profile is related with the interplay between the slope of the stellar mass profile, exponential without any significant change, and that of the gas profile, which is shallower in the inner part and drops rather abruptly beyond the break radius. The shallow inner profile of the gas can be attributed to angular momentum transfer from the inner particles towards the outer parts, possibly due to spiral arm instabilities (Kaufmann et al. 2007) or viscosity effects. The steeper profile of the inner stellar disk is likely due to the inside-out grow mode of our disks: the smaller the radius the longer star formation has been going on there. Going from the centre towards the break radius, the ratio of gas mass to stellar mass, and consequently, the ratio of SFR to stellar mass increases. This explains the coincidence of the break radius with the minimum of mean stellar age. Once we reach the break radius, there is a change in the slope of the gas density profile that can be interpreted as an ending of the gas disk. This is likely to be due to cosmological effects such as inflow of gas with angular momentum not aligned with the disk rotation.

Independently of the mechanism that leads to a cutoff of the gaseous disk at large radii, there is a transition zone between the break and the cutoff radius where star formation is still possible, but the slope of the SFR is steeper than that of the stellar disk. There must be a mechanism that brings stars to this area, since star formation alone cannot account for all the stars present there. We have analysed the origin of the stars present in the outer disk ($r > r_b$) at $z = 0$ by tracing them back in time. We divide the volume of each simulation into three regions at $z = 0.9$. We assume a disk height of 2 kpc and define the inner disk as a cylinder with $r < r_b$ and the outer disk as a volume with $r_b < r < r_c$. The rest of the volume is considered to be external. In the top-right panel of Fig.4 we show the fraction of the outer disk stars that belong to each of these volumes, separated also into gas and stars (likely old and moderately old stars at $z = 0$, respectively). As it can be seen, most stars (64–78%) in the outer disk were residing in the inner disk at $z = 0.9$, either as gas (the majority), or stars. This indicates that stellar migrations play a relevant role in the build up of the outer disk, as Roškar et al. (2008a) pointed out. Few of the particles (2–6%) were already present in the outer disk, this is expected since the disk size is significantly smaller at that time, and by no means should be taken as an indication that the present SFR in the outer disk has such a little weight. The rest (20–34%) were located outside of the galaxy either in smaller objects that merged in, either as diffuse gas. The fact that most of the stars in the outer disk originate in the inner disk means that the star formation taking place in the outer disk is sub-dominant when compared with the stars that got transported there by secular processes, possibly driven by spiral arms, or got scattered there in a merger process. In the rest of panels of Fig.4 we show for one of the galaxies the radial distances of different types of particles at $z = 0.9$ versus their corresponding distances at $z = 0$. The bottom-right panel displays stellar particles born before $z = 0.9$ (old-star migrations), while the bottom-left shows particles that become stellar after $z = 0.9$ (younger star progenitor migrations). Finally, in the top-left panel we give results for gas particles. We can clearly see that old stellar particles have migrated to the outer region. The trend for stars born after $z = 0.9$ and with $r <3$ kpc at $z = 0.9$ is even clearer, although these are a minority. Gaseous particles also migrate. We then conclude that such migrations are likely the main origin of the U-shaped age profile and, therefore, of the luminosity break.

We are indebted to Ignacio Trujillo for useful discussions and suggestions and Judit Bakos for kindly providing us their observational data. We also thank the anonymous referees for their helpful comments and suggestions. This work was partially supported by the Ministerio de Ciencia e Innovación, Spain, through grants AYA2006-15492-C03-01 and AYA2006-15492-C03-02 from the PNAyA, and grant CSD-2007-00050 from the Consolider Ingenio-2010 program. It was also supported by the Madrid IV PRICIT program through the ASTROCAM Astrophysics network (S-0505/ESP-0237). We thank the Centro de Computación Científica (UAM, Spain) and the Barcelona Supercomputing Center for computing facilities and support.

REFERENCES

Abadi, M. G., Navarro, J. F., Steinmetz, M., & Eke, V. R. 2003, ApJ, 591, 499, arXiv:astro-ph/0211331
Azzollini, R., Trujillo, I., & Beckman, J. E. 2008, ApJ, 684, 1026, 0805.2259
Bakos, J., Trujillo, I., & Pohlen, M. 2008, ApJ, 683, L103, 0807.2776
Balcells, M., Graham, A. W., & Peletier, R. F. 2007, ApJ, 665, 1104, arXiv:astro-ph/0404381
Barber, C. B., Dobkin, D. P., & Huhdanpaa, H. 1996, ACM Trans. Math. Softw., 22, 469
Bell, E. F., McIntosh, D. H., Katz, N., & Weinberg, M. D. 2003, ApJS, 149, 289
Bournaud, F., Elmegreen, B. G., & Elmegreen, D. M. 2007, ApJ, 670, 237, 0708.0306
Bruzual, G., & Charlot, S. 2003, MNRAS, 344, 1000
de Jong, R. S. et al. 2007, ApJ, 667, L49, 0708.0826
Debattista, V. P., Mayer, L., Carollo, C. M., Moore, B., Wadsley, J., & Quinn, T. 2006, ApJ, 645, 209, arXiv:astro-ph/0509310
Elmegreen, B. G., & Parravano, A. 1994, ApJ, 435, L121+
Erwin, P., Beckman, J. E., & Pohlen, M. 2005, ApJ, 626, L81, arXiv:astro-ph/0505216
Erwin, P., Pohlen, M., & Beckman, J. E. 2008, AJ, 135, 20, 0709.3505
Ferguson, A., Irwin, M., Chapman, S., Ibata, R., Lewis, G., & Tanvir, N. 2007, Resolving the Stellar Outskirts of M31 and M33, ed. R. S. de Jong, 239–+
Foyle, K., Courteau, S., & Thacker, R. J. 2008, MNRAS, 386, 1821, 0803.2716
Freeman, K. C. 1970, ApJ, 160, 811
Gadotti, D. A. 2009, MNRAS, 393, 1531, 0810.1953
Giovanelli, R., Haynes, M. P., Herter, T., Vogt, N. P., Wegner, G., Salzer, J. J., da Costa, L. N., & Freudling, W. 1997, AJ, 113, 22, arXiv:astro-ph/9610117
Governato, F. et al. 2008, ArXiv e-prints, 0812.0379
Governato, F., Willman, B., Mayer, L., Brooks, A., Stinson, G., Valenzuela, O., Wadsley, J., & Quinn, T. 2007, MNRAS, 374, 1479, arXiv:astro-ph/0602351
Kaufmann, T., Mayer, L., Wadsley, J., Stadel, J., & Moore, B. 2007, MNRAS, 375, 53, arXiv:astro-ph/0601115
Martin, C. L., & Kennicutt, Jr., R. C. 2001, ApJ, 555, 301, arXiv:astro-ph/0103181
Martínez-Serrano, F. J., Serna, A., Domínguez-Tenreiro, R., & Mollá, M. 2008, MNRAS, 388, 39, 0804.3766
Pérez, I. 2004, A&A, 427, L17, arXiv:astro-ph/0410250
Pohlen, M., Dettmar, R.-J., Lütticke, R., & Aronica, G. 2002, A&A, 392, 807
Pohlen, M., & Trujillo, I. 2006, A&A, 454, 759, arXiv:astro-ph/0603682
Pohlen, M., Zaroubi, S., Peletier, R. F., & Dettmar, R.-J. 2007, MNRAS, 378, 594, arXiv:astro-ph/0703768
Power, C., & Knebe, A. 2006, MNRAS, 370, 691, arXiv:astro-ph/0512281
Prunet, S., Pichon, C., Aubert, D., Pogosyan, D., Teyssier, R., & Gottloeber, S. 2008, ApJS, 178, 179, 0804.3536
Roškar, R., Debattista, V. P., Quinn, T. R., Stinson, G. S., & Wadsley, J. 2008a, ApJ, 684, L79, 0808.0206
Roškar, R., Debattista, V. P., Stinson, G. S., Quinn, T. R., Kaufmann, T., & Wadsley, J. 2008b, ApJ, 675, L65, 0710.5523
Sanchez-Blazquez, P., Courty, S., Gibson, B., & Brook, C. 2009, ArXiv e-prints, 0905.4579
Serna, A., Domínguez-Tenreiro, R., & Sáiz, A. 2003, ApJ, 597, 878
Shen, S., Mo, H. J., White, S. D. M., Blanton, M. R., Kauffmann, G., Voges, W., Brinkmann, J., & Csabai, I. 2003, MNRAS, 343, 978, arXiv:astro-ph/0301527
Springob, C. M., Masters, K. L., Haynes, M. P., Giovanelli, R., & Marinoni, C. 2007, ApJS, 172, 599
Trujillo, I., & Pohlen, M. 2005, ApJ, 630, L17, arXiv:astro-ph/0507533
van der Kruit, P. C. 2007, A&A, 466, 883, arXiv:astro-ph/0702486

TABLE 1
OBJECTS ANALYZED

Galaxy	m_{bar}[a]	M_{star}[b]	D/T[c]	r_e[c]	r_b[c]	$M_I - 5\log(h)$[d]	h_{z1}[e]	$M_{r,s}$[f]
	ϵ	M_{gas}[b]	r_s[c]	n[c]	r_c[c]	V_{rot}[d]	h_{z2}[e]	$r_{50,s}$[f]
	[$M_\odot$]	[$10^{10} M_\odot$]		[kpc]	[kpc]		[kpc]	
	[kpc]	[$10^9 M_\odot$]	[kpc]		[kpc]	km/s	[kpc]	[kpc]
6795	2.92×10^6	3.86	0.39	0.45	10.75	-20.75	0.50	-20.82
	0.55	9.59	4.42	0.87	18.1	203.6	1.53	2.32
5003	3.82×10^5	1.71	0.67	0.26	9.83	-20.14	0.42	-20.23
	0.40	4.15	2.92	0.91	12.1	133.2	1.99	1.22
5004	3.82×10^5	3.46	0.64	0.31	12.60	-20.78	0.59	-20.88
	0.40	7.25	3.92	2.33	20.2	162.2	2.14	2.66

[a]Mass of a single baryonic particle (gas or star).
[b]This value was computed using the particles inside ten times the disk radius r_s for each object.
[c]r_s is the inner disk scale length or e-folding length. r_e is the effective radius of the bulge. r_b is the break radius. r_c is the cutoff radius. n is the Sérsic parameter for the bulge. The fits are for the r-band luminosity profile, obtained using the models of Bruzual & Charlot (2003).
[d]Total I-band luminosity and gas rotation speed.
[e]Vertical mass profile scaleheights for the thin and thick stellar disks. Obtained using particles with $r_e < r < r_b$.
[f]Sérsic fits to the total light distribution. Given are Sérsic's half-light radius and total r-band luminosity.

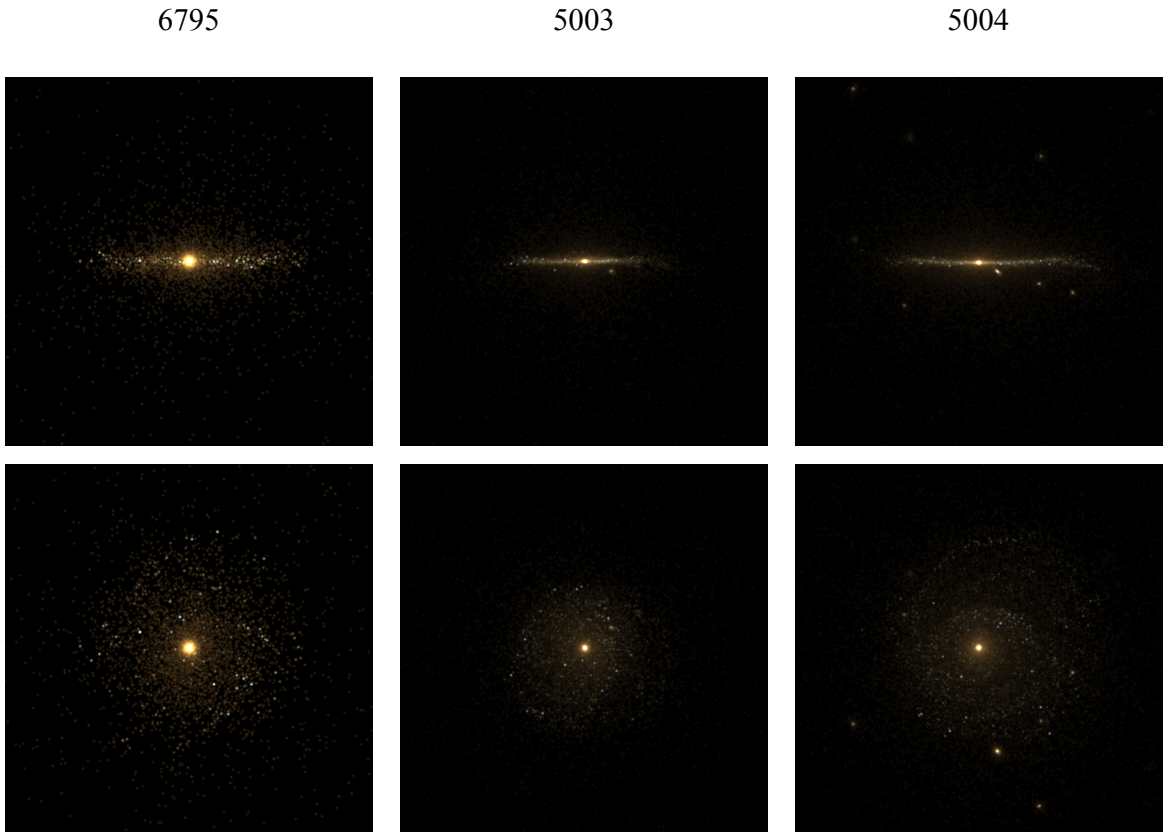

FIG. 1.— Face-on and edge-on synthetic images obtained using Bruzual & Charlot (2003) models. All images are 50 kpc side.

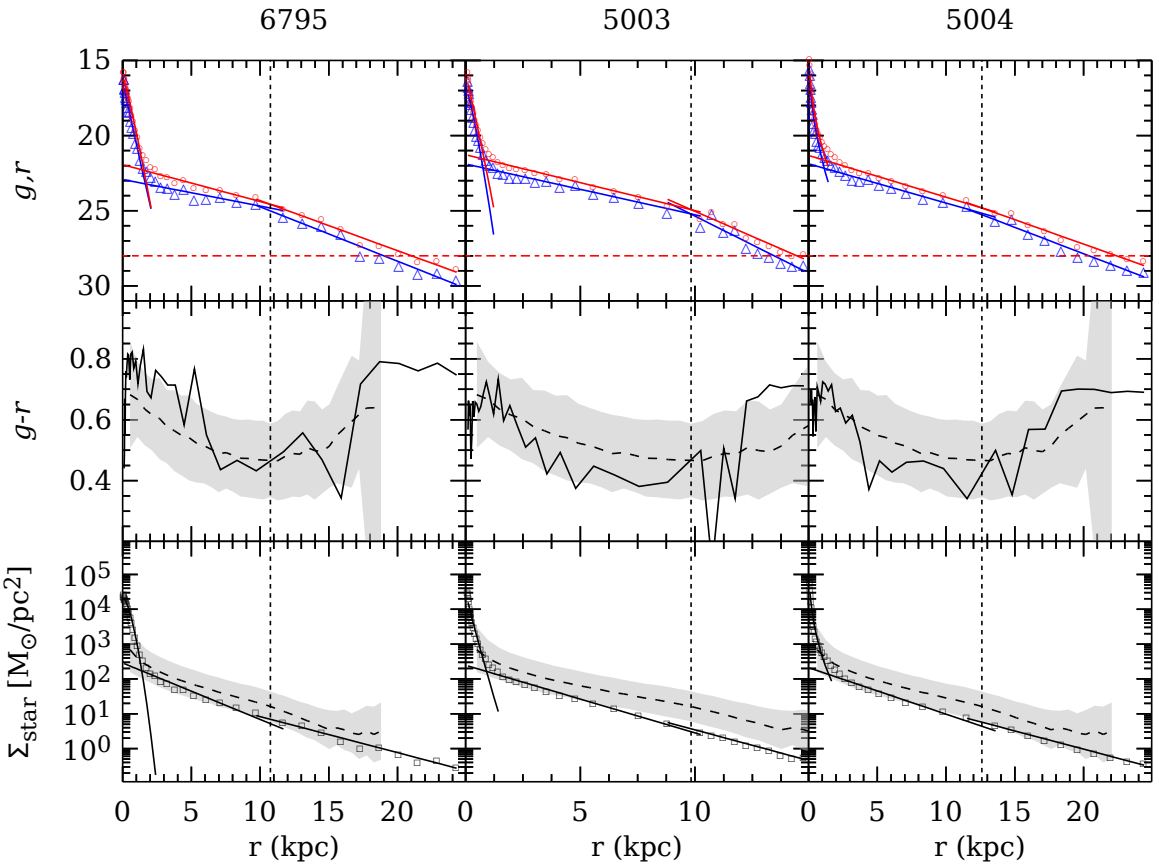

FIG. 2.— Observational properties of the galaxies presented in this letter. The top panels show the face-on luminosity profile for each galaxy in the *r* (circles) and *g* (triangles) bands, together with fits to the bulge and both disk components. Units are mag/□″. The break radius for each galaxy separating the inner and outer exponential components is shown as a dashed vertical line and an approximate critical surface brightness of $\mu_{\rm lim}$ = 28.0 *r*-mag/□″. The middle row shows the *g-r* color profile (compare with Bakos et al. 2008). The bottom row shows the mass profile which unlike the luminosity profile is either exponential anti-trucated. For reference, we have overplotted the Bakos et al. (2008) data for the color and mass plots as dashed lines with the scatter of the observational data shown as a gray shaded area.

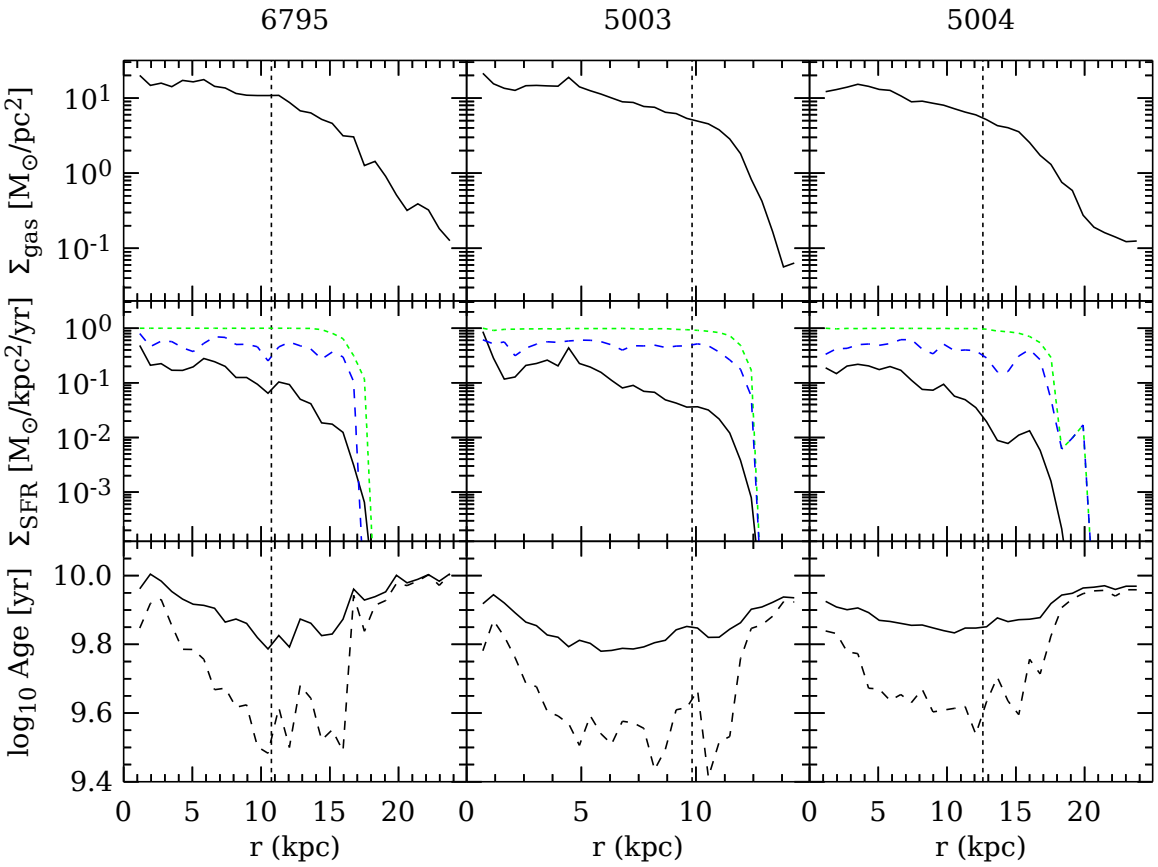

FIG. 3.— Dynamical properties of the galaxies presented in this work as a function of radius. The top panels show the gas column-density profile. As in Figure 2, the dashed vertical line shows the computed break radius for each galaxy in the *r* band. The middle row shows the instantaneous star formation rate derived from the Schmidt law implemented in the code as a continuous line, with the fraction of gas particles able to form stars according to the $\rho_{\rm thres}$ limit and both the $\rho_{\rm thres}$ and $\nabla \cdot \mathbf{v} < 0$ criterion shown as a dotted and dashed lines respectively. The bottom row shows the mean stellar age weighted by stellar mass (continuous line) and *r*-band luminosity (dashed line).

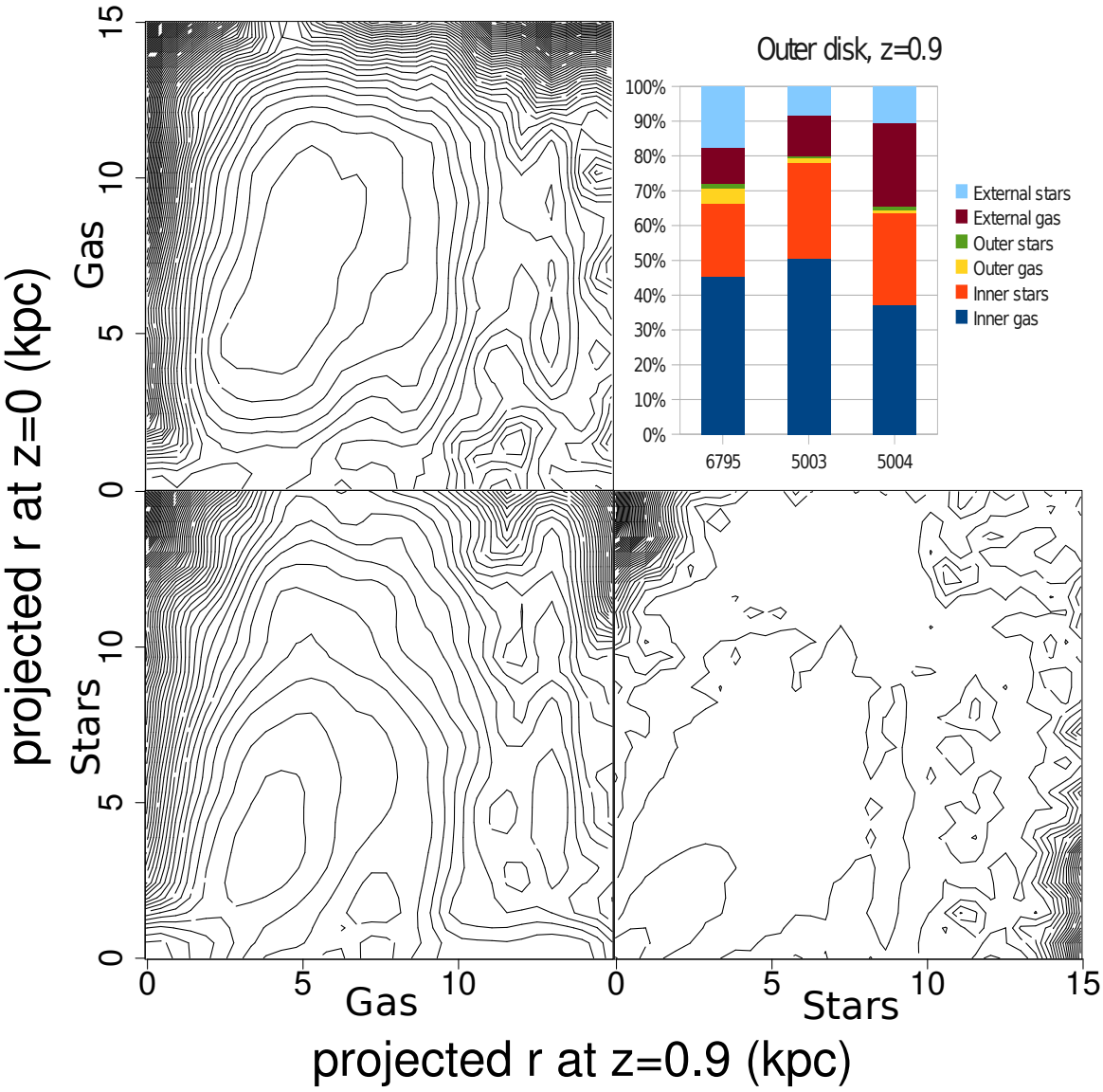

FIG. 4.— Top-right panel: Location at $z = 0.9$ of the outer disk stars at $z = 0$. As an example, the other panels contain contour plots of the evolution of the radial position of particles from $z = 0.9$ to $z = 0$.